Heat and Mass Transfer 37 (2001) 251–257 © Springer-Verlag 2001

Experimental study of optimum spacing problem in the cooling of simulated electronic package

S. Chen, Y. Liu, S. F. Chan, C. W. Leung, T. L. Chan

Abstract An experimental investigation has been performed to determine the effects of different arrangements of obstacles on the cooling of simulated electronic package. The considered simulated electronic package consisted of a channel formed by two parallel plates. The bottom plate is attached with five identical electrically heated square obstacles, which are perpendicular to the mean airflow and arranged with different side-to-side distances. The experimental results show that the conventional equi-spaced arrangement might not be the optimum option and should be avoided. A better thermal performance could be obtained when the side-to-side distances between the obstacles followed a geometric series. For example, at Re = 800, the highest temperature of the optimum arrangement could be reduced by 12% compare to the equi-spaced arrangement and the maximum temperature difference among the five obstacles is lower than that of equi-spaced arrangement by 32.1%.

List of symbols

A	surface area (i.e. top and two sides) of each obstacle exposed to air, m^2
B	obstacle height above the base of the simulated electronic package, m
C	clearance between the upper surfaces of the ribs and the ceiling of the channel, $C = H - B$
E	electric power supplied to each obstacle, W
F	view factor for thermal radiation from an obstacle to its surroundings
h	convective coefficient for heat transfer from an obstacle to the airflow, $W/(m^2 \cdot K)$
H	vertical free height within the unencumbered duct, m
k	thermal conductivity of the fluid, $W/(m \cdot K)$
Nu	Nusselt number
Pr	Prandtl number, ν/α
Q	steady-state rate of heat loss from the simulated electronic package, W
Re	Reynolds number, UC/ν
T	temperature, K
U	mean air speed in the duct, m/s
α	thermal diffusivity
ε	mean surface emissivity with respect to thermal radiation
ν	kinematic viscosity of the fluid, m^2/s
σ	Stefan–Boltzmann constant, $W/(m^2\ K^4)$

Subscripts

a	airflow
ave	average value
c	forced convection
i	ambient environment
l	conduction
n	number of obstacle
r	via thermal radiation
s	the obstacle's surface

1 Introduction

The electronic devices miniaturization is characterized by high rate of heat dissipation per unit of component area and it demands the electronic system has enough heat dissipation capability in order to avoid its temperature from rising significantly, which may lead to malfunction and breakdown of the entire device. Improvements of cooling techniques are crucial to meet the design and development of rather complex circuits and dense electronic boards.

Fluid flow around obstacles mounted on a channel wall forms a fundamental basis for studies of the cooling of electrical devices. Mixed convection in horizontal channels is of interest in cooling of local heat sources encountered in electronic devices. Investigations of the cooling of electronic components have been widely studied both numerically and experimentally (Incropera, [1]).

Kennedy and Zebib [2] reported mixed convection between horizontal parallel plates with a local heat source flash-mounted on the horizontal plate. They showed the heat transfer characteristics and flow pattern resulting from four cases of heat source locations. Incropera et al. [3–5] has performed a series of numerical and experimental studies in a rectangular horizontal channel. Mixed convection in the entrance region was extensively discussed, and they visualized four flow regimes along the bottom plate-laminar, mixed, transitional, and turbulent regimes. Consequently, significant improvement in heat transfer was found to be due to the buoyancy-driven

Received on 17 December 1999

S. Chen, Y. Liu (✉), S. F. Chan, C. W. Leung, T. L. Chan
Department of Mechanical Engineering
The Hong Kong Polytechnic University
Hung Hom, Kowloon, Hong Kong

Support given by The Hong Kong Polytechnic University under Central Research Grant No. G-YB87 is gratefully acknowledged.

secondary flow. Kang et al. [6] investigated experimentally mixed convective transport from an isolated source located on a horizontal adiabatic plate. The dependence of the heat transfer rate on the mixed convection parameter and on the thickness of the heated element was investigated. However, the effect of thermal wake interaction could not be clarified because single heat source configurations were considered. Bratten and Patankar [7] studied numerically the laminar mixed convection in shrouded arrays of heated rectangular blocks mounted on the horizontal shrouds, spaced periodically in the spanwise direction. Kim et al. [8] presented numerical results on the mixed convection from multiple-layered boards with cross-streamwise periodic boundary conditions in a horizontally-oriented channel and a vertically-oriented channel. Papanicolaou and Jaluria [9] investigated conjugate mixed convection from a discrete thermal source or multiple sources in a rectangular cavity. They observed that the location of the source on the right vertical wall is the most favorable in terms of cooling, and that oscillatory flow and thermal fields could develop in the enclosure depending on the relative location of the components at high inputs by the components. Elpidorou et al. [10] investigated mixed convection in a vertical channel with a finite wall heat source, and their results revealed the fundamental nature of mixed convection in a vertical channel. The effects of inclination angle on the flow and heat transfer characteristics under buoyancy-assisting flow conditions have been studied by Naito and Nagano [11] in the entrance region between parallel plates and Lin et al. [12] in a duct with a backward facing step. Both studies indicated that the inclination angle could play an important role in the velocity and temperature fields. Shaw et al. [13] studied mixed convection phenomena with an isothermal heating block in a three-dimensional channel. Papanicolaou and Jaluria [14, 15] extensively studied two-dimensional conjugate mixed convection from a localized heat source in a cavity with two openings. Oscillatory results were observed beyond the critical value of Gr/Re^2, and the results were initially characterized by a single frequency. As Gr/Re^2 increased further, the oscillations showed irregular patterns that indicated the flow was approaching the turbulent regime. Choi and Ortega [16] numerically studied the effects of laminar forced flow on buoyancy-induced natural convection cells throughout the regions of natural, mixed and forced convection for a parallel plane channel with a discrete heat source. They found that there was no significant penalty in heat transfer due to the inclination of the channel up to 45°. Huang and Lin [17] numerically investigated the unsteady and transitional characteristics of mixed convection flows of air in a three-dimensional channel. The evolution of these complicated flows was discussed in detail. Mixed convection in a semicircular duct with an axially non-uniform boundary condition on a flat wall has been numerically studied by Karki et al. [18]. The study showed the significant effect of the thermal boundary condition along the curved wall on the secondary flow pattern and, therefore, on the heat flux distribution on the heat transfer surface. Leung et al. [19] studied the convective heat transfer in a rectangular duct flow with streamwise-periodic rectangular heated ribs mounted one of the principal walls, which simulated a printed-circuit board assembly. Effects of varying the duct's height, and the rib's height and width on convection from the rib's surface to the airflow were presented. Choi and Kim [20] numerically investigated the three-dimensional conjugate mixed convection in a channel. They proposed a 'modified 5% deviation rule' to define the natural, mixed and forced convection regimes and found an important role of conductive board in determining the heat transfer mode.

In most of the problems considered, it has been common practice that an equi-spaced arrangement of heated components was assumed. Nevertheless, due to the thermal interaction among heated components, the equi-spaced arrangement might not be the optimum option, and there must be an optimum spacing arrangement among the electronic components. Here, the optimum arrangement is defined as that which yields the lowest maximum temperature and minimizes the temperature differences among the components.

Liu et al. [21] [22] numerically studied the optimum spacing problem for five chips on a horizontal substrate in natural convection, it was found when the chips were arranged in geometric series, the maximum temperature could be reduced more than 10%. The best arrangement was found when the geometric ratio was Golden Mean.

In this paper, we focus on the experimental aspects of the optimum spacing problem in mixed convection and forced convection. Five heated obstacles are rested on a horizontal substrate with different spacing ratios in a channel, and the air passes through it. The main objective is to investigate the influence of spacing ratio on the cooling of electronic packages and to provide the optimum thermal design.

2 Experimental apparatus

The schematic view of the experimental system is shown in Fig. 1. The experimental apparatus is operated in suction mode and oriented horizontally. The system consists of 5 upward-facing rectangular copper obstacles, which are mounted on a smooth board (as shown in Fig. 2). The whole system is placed horizontally. The heated obstacles, which are used to simulate the thermal behavior of the electronic components, are highly polished in order to achieve a low surface emissivity of less than 0.3 (as indicated by a Minolta 505 infrared spot thermometer). Each obstacle has a length of 200 mm and a height of 6.35 mm. Two 0.8 Ω nichrome heater strips are embedded in the base of each copper obstacle to provide a uniform heat flux. Electric power supplied to the obstacles is adjusted via a variable-voltage transformer and recorded by a digital wattmeter. Since the nichrome strips could achieve 99% efficiency, nearly all the electric power supplied to the heater strips is therefore converted to heating power. K-type thermocouple is embedded in a narrow central slot in the upper surface of every obstacle, and the thermocouple signals are converted to temperature readings via a Diqi-sense digital thermometer. Each thermal junction is formed by spot welding. Good thermal contact between the thermal

junction and the obstacle is ensured by filling the residual cavity with heat transfer compound. This method enabled the point of measurement to be placed closer to the inner surface of the slot of the obstacle where the temperature reading is more preferable, such that leading to a more accurate temperature measurement. The simulated electronic package is 200 mm wide and formed by fixing a 2 mm thick mica sheet to a 6.35 mm thick bakelite substrate, and the undersurface of which is covered with a layer of glass fiber. The board is machined to have sharp leading and trailing edges. The simulated electronic package is placed symmetrically in the wind tunnel's rectangular test section (length 600 mm, cross-section dimension 202 × 120 mm) made of 6.35 mm thick bakelite sheet. The whole test section except the upper plate is thermally insulated from its surroundings by a 50 mm thick glass fiber layer, the upper plate is exposed to the air. The internal height of the wind tunnel is fixed at 0.03 m for the present investigation.

Ambient air (Pr = 0.7) passes through the wind tunnel via an electric blower. The blower is physically isolated from the wind tunnel in order to avoid the transmission of vibration from the blower to the duct. Since the experiments are performed with different flow conditions, the electric power supplied to drive the blower is adjusted through a variable-voltage transformer so as to obtain different mean airflow velocity. The airflow velocity is measured with a Kurz 441 M hot-wire anemometer. The steady-state temperatures of the airflow at the entrance and exit of the test section are measured by a K-type long-probe thermocouple connected with the digital thermometer. The diameter of the long probe thermocouple is only 1.5 mm so that it would not affect the flow pattern significantly during each measurement. In addition, all connecting parts are added with gaskets and seals to prevent air leakage and soap bubble is used to test any air leakage at each point.

A total of 5 different arrangements are considered and the geometric parameters are listed in Table 1. S_1 is the side-to-side distance between obstacle #1 and obstacle #2, S_2 the side-to-side distance between obstacle #2 and obstacle #3, S_3 the side-to-side distance between obstacle #3 and obstacle #4, S_4 the side-to-side distance between obstacle #4 and obstacle #5, and S_5 the side-to-side distance between obstacle #1 and obstacle #5. In the present study, S_5 is fixed at 133.35 mm.

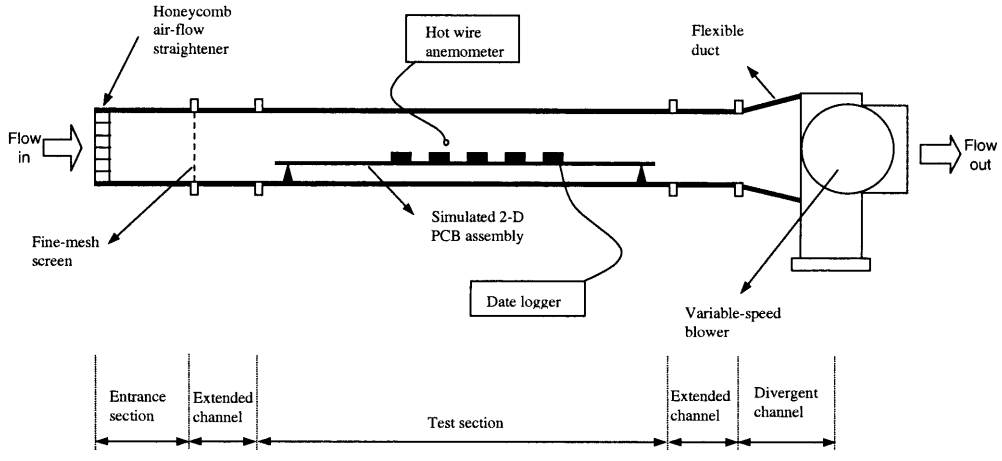

Fig. 1. The geometry of parallel plate channel with five heated obstacles

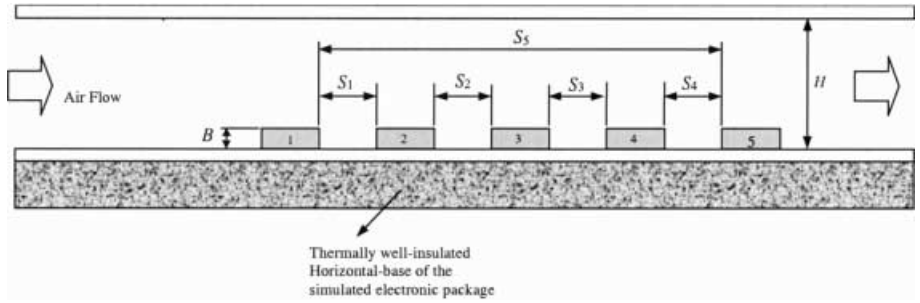

Fig. 2. Test geometry of the simulated electronic package

Table 1. Geometry arrangement

Type	S_1 (mm)	S_2 (mm)	S_3 (mm)	S_4 (mm)	Geometric relation
1	19.05	19.05	19.05	19.05	$S_4/S_3 = S_3/S_2 = S_2/S_1 = 1.0$
2	8.23	13.17	21.08	33.72	$S_4/S_3 = S_3/S_2 = S_2/S_1 = 1.6$
3	5.08	10.16	20.32	40.64	$S_4/S_3 = S_3/S_2 = S_2/S_1 = 2.0$
4	11.08	17.72	28.35	19.05	$S_3/S_2 = S_2/S_1 = 1.6$, $S_4 = 19.05$ mm
5	8.16	16.33	32.66	19.05	$S_3/S_2 = S_2/S_1 = 2.0$, $S_4 = 19.05$ mm

3
Handling of the experimental data

The steady-state convection heat loss from each obstacle to the airflow is obtained by:

$$Q_c = E - Q_r - Q_l \tag{1}$$

The conduction loss (Q_l) from the obstacle to the attached rectangular plate is estimated by using Fourier's law with knowledge of the thermal conductivity of the board material and the measured associated temperature distribution. The rate of radiation loss (Q_r) from an obstacle to its environment is assessed by the following equation:

$$Q_r = \sigma A F \varepsilon (T_s^4 - T_i^4) \tag{2}$$

where the view factor (F) between the obstacle and its surroundings, is taken to be unity and the surface emissivity is measured to be 0.3. After Q_l and Q_r (which are estimated to be approximately 4 and 6% of E, respectively) are deduced from E, the value of (Q_c) could be determined. Then the convective heat transfer coefficient from the nth obstacle to the airflow is obtained from the definition:

$$h_n = \frac{Q_c}{A(T_s - T_a)} \quad n = 1 \sim 5 \tag{3}$$

The steady-state temperature of airflow (T_a) is assumed to vary linearly from inlet to exit of the test section, and its mean value is used as the reference temperature to determine the values of the air's properties applicable for the investigation. The average heat transfer coefficient over the entire simulated electronic package could be obtained from:

$$h_{ave} = \tfrac{1}{5}\sum_{1}^{5} h_n \tag{4}$$

The vertical clearance of the simulated electronic package ($C = H - B$) is chosen as the characteristic dimension to define the Reynolds and Nusselt numbers, i.e.

$$Re_c = \frac{U \cdot C}{v} \tag{5}$$

$$Nu_c = \frac{h_{ave} \cdot C}{k} \tag{6}$$

4
Heat transfer results

Figure 3 shows the surface temperature of each obstacle of TYPE 1 arrangement at different Reynolds numbers. TYPE 1 is an equi-spaced arrangement, which is commonly employed in the cooling of electronic packages at present. When the air flowed from the inlet to the outlet of the channel, it is heated by the obstacles step by step. In this case the minimum temperature occurred at obstacle #1 while the maximum temperature occurred at obstacle #3. The temperature of obstacle #3 is much higher than that of obstacle #1 (nearly 32% when the Reynolds number is 265). As obstacle #4 and obstacle #5 are near from the outlet of the channel, due to the "exit" effect, their temperatures are lower than that of obstacle #3.

Figure 4 shows the temperature of each obstacle of TYPE 2 arrangement at different Reynolds numbers. For

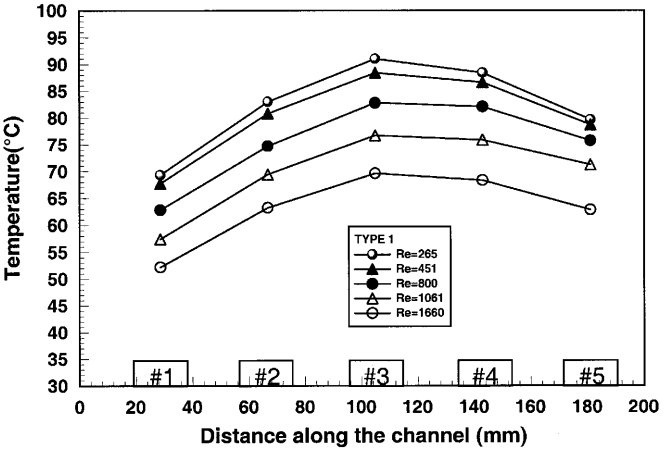

Fig. 3. Surface temperature of each obstacle of TYPE 1 arrangement

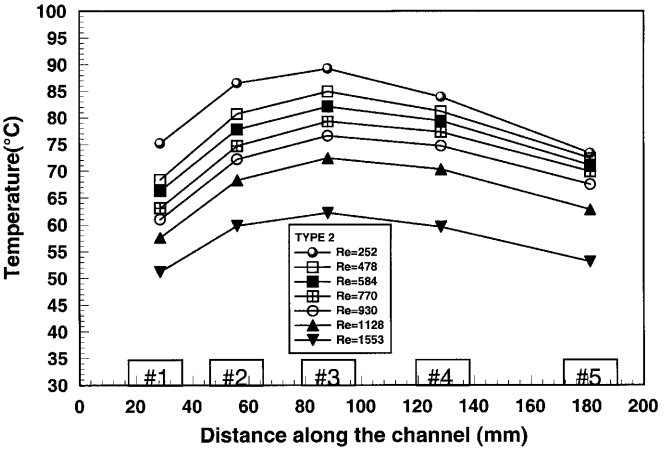

Fig. 4. Surface temperature of each obstacle of TYPE 2 arrangement

TYPE 2, the side-to-side distance between obstacles followed the geometric ratio, and the geometric ratio is 1.6, i.e. $S_4/S_3 = S_3/S_2 = S_2/S_1 = 1.6$. As the side-to-side distance between obstacle #1 and obstacle #5 is unchanged ($S_5 =$ constant), S_1 is reduced while S_4 is increased compared to that of TYPE 1 arrangement. This results in the decrease of temperature difference between obstacle #1 and obstacle #2 and the increase of temperature difference between obstacle #4 and obstacle #5. The maximum temperature occurs at obstacle #3. The temperature difference between obstacle #1 and obstacle #5 is smaller than that of TYPE 1 arrangement.

Figure 5 shows the temperature of each obstacle of TYPE 3 arrangement at different Reynolds numbers. For TYPE 3 arrangement, the side-to-side distance between obstacles followed the geometric ratio of 2.0, i.e. $S_4/S_3 = S_3/S_2 = S_2/S_1 = 2.0$. Due to the thermal interaction, the lowest temperature occurs at obstacle #5 instead of obstacle #1, compared to TYPE 1 and TYPE 2 arrangements. The temperature of obstacle #5 decreases due to the increase of the side-to-side distance between obstacle #4 and obstacle #5. Furthermore, the temperature distribution among the

obstacles of TYPE 3 is different from those of TYPE 1 and TYPE 2 arrangements.

Figures 4 and 5 show if the side-to-side distances followed the geometric ratio, it would enlarge the distance between the last two obstacles and increase the temperature difference between these two obstacles. As a result, the minimum temperature occurred at obstacle #5 instead of obstacle #1. Hence a new arrangement is considered. Figure 6 shows the temperature of each obstacle of TYPE 4 arrangement at different Reynolds numbers. For TYPE 4 arrangement, the distance S_4 is fixed and is the same as that of TYPE 1 arrangement, but $S_3/S_2 = S_2/S_1 = 1.6$. The temperature difference between different obstacles is decreased and the lowest temperature occurred at obstacle #1. Figure 7 shows the temperature of each obstacle of TYPE 5 arrangement at different Reynolds numbers. For TYPE 5 arrangement the distance S_4 is the same as that of TYPE 1 arrangement while $S_3/S_2 = S_2/S_1 = 2.0$. The lowest temperature occurs at obstacle #1 whereas for TYPE 3 the lower temperature occurred at obstacles #5. When Reynolds number is low (Re = 252) the maximum temperature occurred at obstacle #2. The temperature difference between obstacle #2 and obstacle #3 is very small.

Figure 8 shows the maximum temperature of different types of arrangements among the five obstacles with the Reynolds numbers. All the maximum temperatures decrease with increasing Reynolds numbers. When Reynolds number is 800, the maximum temperature is 83 °C for TYPE 1, 79 °C for TYPE 2 and 87 °C for TYPE 3. It can be found that when the arrangement of the obstacles followed the geometric ratio of 1.6, the maximum temperature decreased and it is reduced by about 4.8% compared to TYPE 1 arrangement. When the geometric ratio is further increased, i.e. for Type 3 arrangement the ratio is 2.0, its maximum temperature is about 4.8% higher than that of TYPE 1 arrangement. Furthermore, for TYPE 4 arrangement, the ratio is 1.6 and S_4 is fixed at 19.05 mm, the maximum temperature is 73 °C, which decreases significantly and is reduced by 12% (10 °C) compared to TYPE 1 arrangement. From the thermal design point of view, it is a better option. For TYPE 5 arrangement, its maximum temperature increased slightly compared to TYPE 4 arrangement.

Figure 9 shows the maximum temperature difference among these 5 obstacles for TYPE 1 to TYPE 5 arrangements. When Reynolds number is 800, for TYPE 1 the

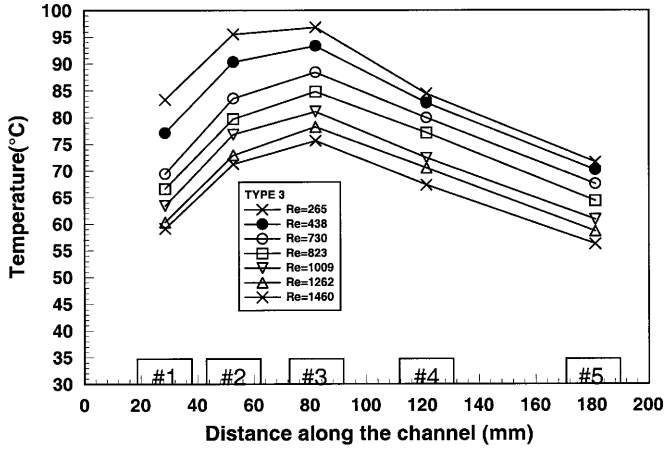

Fig. 5. Surface temperature of each obstacle of TYPE 3 arrangement

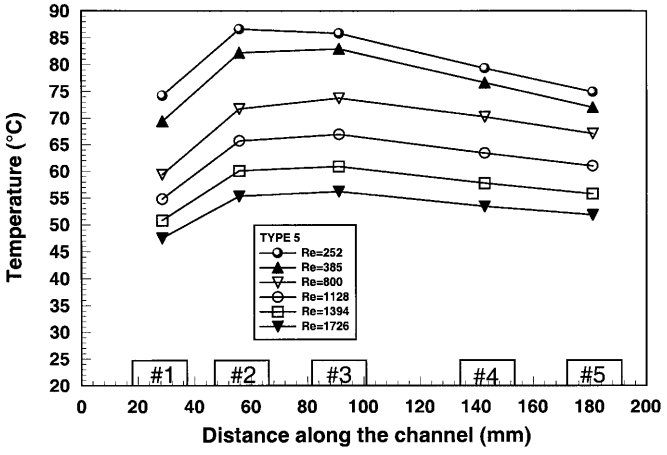

Fig. 7. Surface temperature of each obstacle of TYPE 5 arrangement

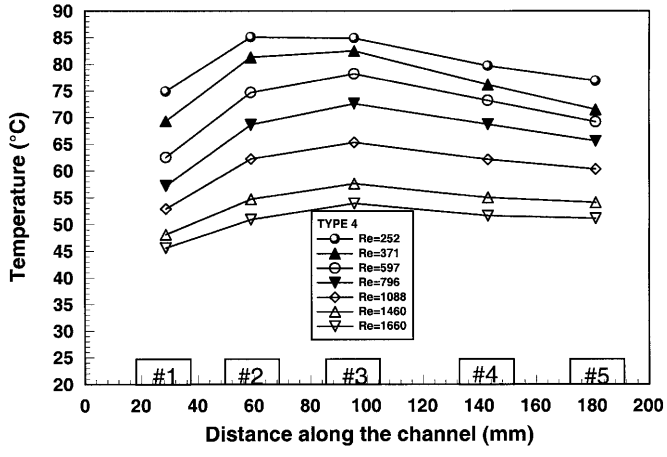

Fig. 6. Surface temperature of each obstacle of TYPE 4 arrangement

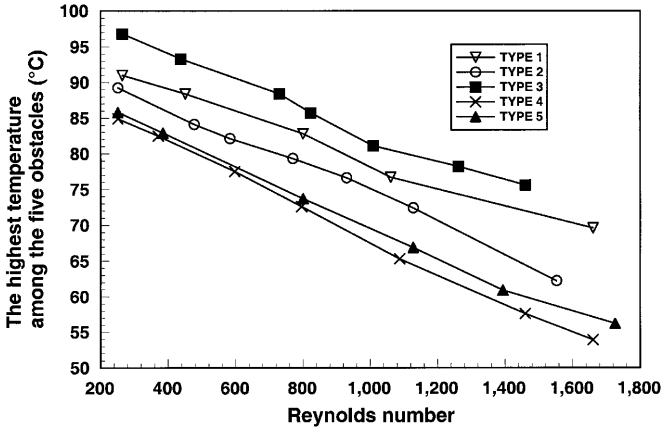

Fig. 8. The highest temperature of different types of arrangements among the five obstacles with different Reynolds numbers

maximum temperature difference is 23 °C. For TYPE 2 arrangement, it is 16.4 °C, which is lower than that of TYPE 1 arrangement by 28%. For TYPE 3 arrangement, its maximum temperature difference is 25 °C, which is larger than that of TYPE 1 arrangement. For TYPE 4 and TYPE 5 arrangements, the maximum temperature difference is 15.6 and 14.4 °C respectively when Re is 800, which is significantly lower than that of TYPE 1 arrangement by 32.1 and 37.4%, respectively.

Figure 10 shows the variation of the heat transfer coefficient of the individual copper obstacle of TYPE 1 arrangement. It can be found that the steady-state convective heat transfer is relatively greater at the first obstacle and thereafter decreased for obstacle #2 and obstacle #3. However, an increase in heat transfer coefficient occurs at the last two obstacles, this is due to the 'exit' effect (i.e. sudden enlargement of the flow aperture soon after obstacle #5), which leads to an enhanced local flow around obstacle #4 and obstacle #5. Figure 11 shows the variation of the heat transfer coefficient of the individual copper obstacle of TYPE 4 arrangement and it has the same variation as that of TYPE 3 arrangement.

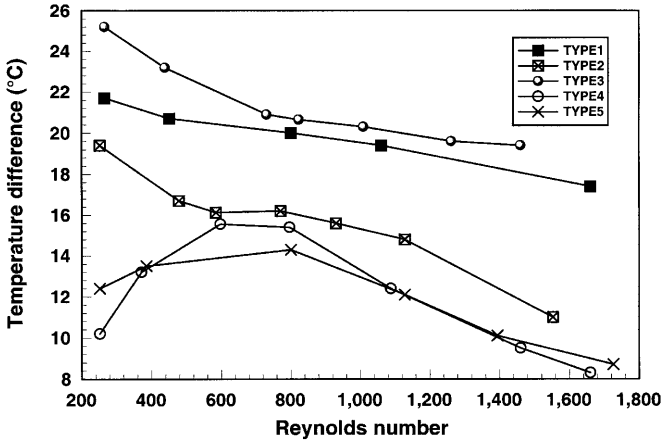

Fig. 9. The maximum temperature difference among the five obstacles for TYPE 1–5 arrangement

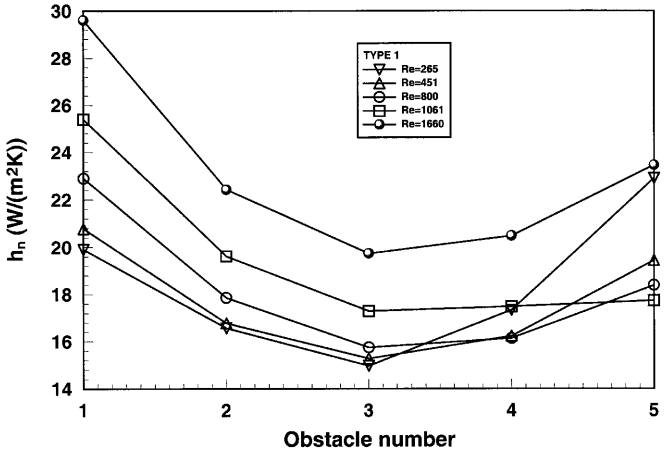

Fig. 10. The heat transfer coefficient of the individual obstacle of TYPE 1

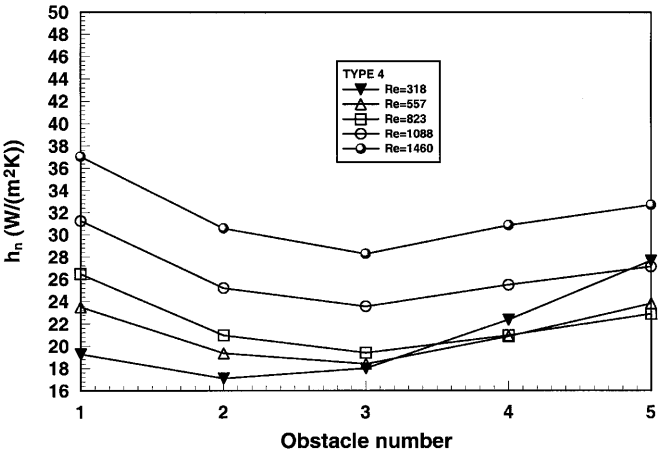

Fig. 11. The heat transfer coefficient of the individual obstacle of TYPE 4

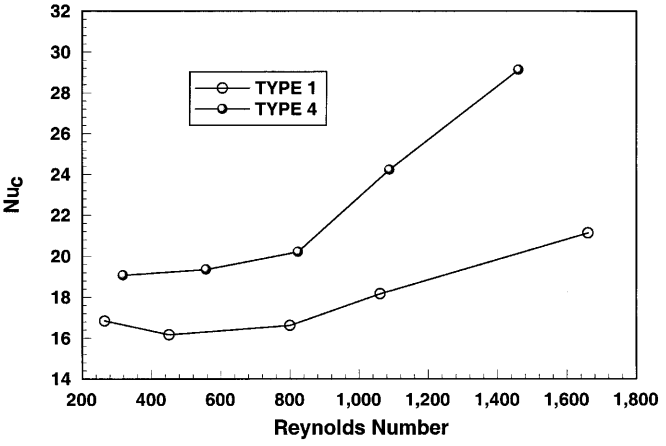

Fig. 12. The variation of average Nusselt number with different Reynolds numbers

Figure 12 shows the averaged Nusselt number versus Reynolds number of the airflow. It is not surprising that the Nusselt number increases with the increasing Reynolds number. For TYPE 4 the averaged Nusselt number is greater than that of TYPE 1 arrangement for all Reynolds number. For example, when Re is 800, for TYPE 1 the averaged number is 17 while for Type 4 arrangement it is 20, which is 17.6% higher than that of TYPE 1 arrangement.

5 Conclusions

An experimental study of optimum spacing problem under steady-state condition in the cooling of electronic packages has been performed. The conclusions are described as follows:

1. The conventional equi-spaced arrangement is not an optimum option for the cooling of electronic packages. The temperature distribution strongly depended on the spacing arrangements.

2. When the side-to-side distances of obstacles followed the geometric series arrangements, different thermal performances could be obtained. If the ratio is 1.6, the max-

imum temperature and the maximum temperature difference among the five obstacles could be decreased significantly. But when the ratio is further increased to 2.0, an opposite trend is observed that both the maximum temperature and the maximum temperature difference among the five obstacles are increased.

3. When the side-to-side distance between the last two obstacles are fixed while others followed the geometric series arrangement, a much better thermal performance could be obtained. For example, when Reynolds number is 800 the maximum temperature in the optimum arrangement (TYPE 4) could be as much as 88% of the equi-spaced arrangement and the maximum temperature difference is lower than that of equi-spaced arrangement by 32.1%.

References

1. **Incropera FP** (1988) Convection heat transfer in electronic equipment cooling. J Heat Transfer 110: 1097–1111
2. **Kennedy KJ; Zebib A** (1983) Combined free and forced convection between horizontal parallel plates: some case studies. Int J Heat Mass Transfer 26: 471–474
3. **Mahaney HV; Incropera FP; Ramadhyani S** (1990) Comparison of predicted and measured mixed convection heat transfer from an array of discrete sources in a horizontal rectangular channel. Int J Heat Mass Transfer 33: 1233–1245
4. **Maughan JR; Incropera FP** (1990) Regions of heat transfer enhancement for laminar mixed convection in a parallel plate channel. Int J Heat Mass Transfer 33: 555–570
5. **Maughan JR; Incropera FP** (1991) Use of vortex generators and ribs for heat transfer enhancement at the top surface of a uniformly heated horizontal channel with mixed convection flow. ASME J Heat Transfer 113: 504–507
6. **Kang BH; Jaluria Y; Tewari SS** (1988) Mixed convection air cooling of an isolated rectangular heat source module on a horizontal plate. ASME Proc Nat Heat Transfer Conf, 59–66
7. **Bratten ME; Patankar SV** (1980) Analysis of laminar mixed convection in shrouded arrays of heated rectangular blocks. Int J Heat Mass Transfer 28: 1699–170
8. **Kim SY; Sung HJ; Hyun JM** (1992) Mixed convection from multiple-layered boards with cross-streamwise periodic boundary conditions. Int J Heat Mass Transfer 35: 2941–2952
9. **Papanicolaou E; Jaluria Y** (1991) Forced and mixed convective cooling of multiple electronic components in an enclosure. Proc ASME/AIChE Nat Conf HTD-171, 29–37
10. **Elpidorou D; Prasad V; Modi V** (1991) Convection in a vertical channel with a finite wall heat source. Int J Heat Mass Transfer 34: 573–578
11. **Naito E; Nagano Y** (1989) Combined forced and free upward-flow convection in the entrance region between inclined parallel plates. ASME J Heat Transfer 111: 675–682
12. **Lin JT; Armaly BF; Chen TS** (1991) Mixed convection heat transfer in inclined backward-facing step flow. Int J Heat Mass Transfer 34: 1568–1571
13. **Shaw HJ; Chen WL; Chen CK** (1991) Study on the laminar mixed convective heat transfer in three-dimensional channel with a thermal source. ASME J Electron Packaging 113: 40–49
14. **Papanicolaou E; Jaluria Y** (1992) Transition to a periodic regime in mixed convection in a square cavity. J Fluid Mech 239: 489–509
15. **Papanicolaou E; Jaluria Y** (1993) Mixed convection from a localized heat source in a cavity with conducting walls: a numerical study. Num Heat Transfer, Part A 23: 463–484
16. **Choi CY; Ortega A** (1993) Mixed convection in an inclined channel with a discrete heat source. Int J Heat Mass Transfer 36: 3119–3134
17. **Huang CC; Lin TF** (1994) Buoyancy induced flow transition in mixed convective flow of air through a bottom heated horizontal rectangular duct. Int J Heat Mass Transfer 37: 1235–1255
18. **Karki KC; Sathyamurthy PS; Patankar SV** (1994) Laminar mixed convection in a horizontal semicircular duct with axially nonuniform thermal boundary condition on the flat wall. Num Heat Transfer, Part A 25: 171–189
19. **Leung CW; Kang HJ** (1998) Convective heat transfer from simulated air-cooled printed-circuit board assembly on horizontal or vertical orientation. Int Comm Heat Mass Transfer 25: 67–80
20. **Choi CY; Kim SJ** (1996) Conjugate mixed convection in a channel: modified five percent deviation rule. Int J Heat Mass Transfer 39: 1223–1234
21. **Liu Y; Leung CW; Chan TL; Phan-Thien N** (1999) An optimum spacing problem for five chips on a horizontal substrate in an enclosure – Natural Convection. Int J Comput Eng Sci (in press)
22. **Liu Y; Phan-Thien N; Leung CW; Chan TL** (1999) An optimum spacing problem for five chips on a horizontal substrate in a vertically insulated enclosure. Comput Mech 24: 310–317